Published in IET Radar, Sonar and Navigation
Received on 3rd December 2012
Revised on 24th July 2013
Accepted on 6th September 2013
doi: 10.1049/iet-rsn.2013.0141

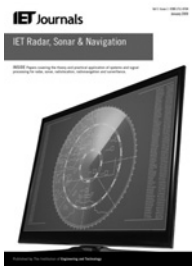

ISSN 1751-8784

Calibration of antenna pattern and phase errors of a cross-loop/monopole antenna array in high-frequency surface wave radars

Hao Zhou, Biyang Wen

School of Electronic Information, Wuhan University, Wuhan 430072, People's Republic of China
E-mail: zhou.h@whu.edu.cn

Abstract: High-frequency surface wave radar has now been widely used as a regular instrument in remote sensing of sea states. To solve the contradiction of the array pattern beamwidth and array aperture, multiple cross-loop/monopole (CM) antennas are used as sub-arrays to form a uniform linear array, which is called the CM-uniform linear array (ULA). Adaptive beamforming via virtual interferences is used to synthesize the desired pattern and a half beamwidth of about 20° is achieved by a two-unit CM-ULA with a spacing of 0.75λ (λ is the radar wavelength). A novel iterative method is proposed to calibrate the array errors, including the individual antenna pattern distortions and the channel gain/phase errors, without resorting to any known signals such as a beacon or transponder signal. Simulations are executed and the results show the validity of the proposed method.

1 Introduction

High-frequency surface wave radar (HFSWR) has now been widely used, and playing important roles, in remote sensing of sea states, such as sea surface currents, winds and waves [1–4]. These data products are quite helpful in many fields, including oceanographic and meteorological researches, early-warning of tsunami, monitoring of oil spills and falling objects from ships and so on. There exist two types of antenna array, that is, phase controlled array (e.g. a uniform linear array (ULA)) and amplitude controlled array (e.g. a cross-loop/monopole array (CMA) [5]). For practicability reasons, small-aperture arrays are preferred and now used in a large portion of the HFSWR operated worldwide to accomplish direction finding (DF) instead of beamforming (BF) to resolve the directions of arrival (DOA) of the sea echoes. The SeaSonde [5, 6] and Wellen radar [7, 8] are two of the most successful commercialised products for sea state monitoring, and they use two distinct antenna array types. The SeaSonde is well known for its special compact 3-element antenna which consists of two cross-loops and one monopole with a common phase centre, whereas the WERA uses a 16- or 12-element ULA for extraction of sea currents, winds and waves and a 4-element square array for sea current extraction only. In the CMA, the orthogonal antenna patterns play the roles of the electronic phases introduced by different element displacements in the ULA to realise the angular resolution, which is often a vital factor for the final data quality. Lots of 'in situ' comparison experiments have been done to validate the radars' sea state extraction performances. However, there are still contradictions between the radar's angular resolving capability and the array aperture in actual applications. To monitor the sea waves over a wide angular area, the CMA and the 4-element square array might be incompetent and the array capable of forming narrow beams (like the 16-element ULA) is preferred. Therefore we always hope to achieve the narrowest beamwidth by a given array aperture since the field for the antenna array is often invaluable. Herein, we combine the CMA and ULA together, using each CMA as one sub-array to form a small-aperture ULA, and call it CM-based ULA (CM-ULA). The advantages of the combination for directional pattern synthesis are obvious: (i) a narrower mainlobe beamwidth is obtained than that achieved by the same aperture filled with monopole elements; (ii) the spacing of the CMA sub-array can be set greater than a half wavelength without generating strong grating lobes; and (iii) the front/back ambiguity of the ULA can be greatly decreased because of the increased front-to-back ratio. To further decrease the mainlobe beamwidth and lower the sidelobes, the adaptive BF (ABF)-based algorithm [9] is used for the array pattern synthesis. The weight vector is firstly assigned to be the steering vector of the array, corresponding to a spatial-domain matched filter, and then it is iteratively refreshed to drive the pattern to approach to the desired one by adjusting the virtual interferences, which are uniformly spaced throughout the look angles. This method is found to be very convenient to realise for our application.

Besides the array configuration and pattern synthesis algorithm, the calibration of the gain and phase errors of the antennas is also an important problem. Errors in mutual coupling, antenna positions and channel gain/phase variations are known to degrade array performance. For HFSWR radar with a CM-ULA, the cross magnetic loops are encapsulated in a small box (typically 20 cm × 20 cm)

and the monopole is normally shorter than one-tenth of the wavelength, so the mutual coupling is negligible. The antenna position errors can also be neglected as the positions can be easily and accurately measured in such a small-aperture array considered here. Lots of research work has been put forward in calibration of array errors, including use of known and unknown sources [10–15]. The use of known signals incident from the far field (e.g. a beacon or transponder signal) provides a simple and direct way to estimate the errors, but such signals are not always available and the active circuit components in the loop antennas and radar receiver may be susceptible to the variations of the environment and temperatures. So, the use of unknown sources may be a better choice to track the variations of the array errors. The existing self-calibration methods generally deal with arrays consisting of antennas with the same patterns, which are unsuitable for the solution of our problem. It is noteworthy that the phase errors of a linear array cannot be absolutely calibrated, but when cross-loops are involved the ambiguity can be eliminated because of the extra direction-dependent amplitude information.

One more important problem in the CM-ULA is that the distortions of individual antenna patterns also degrade the array performance. The antenna pattern satisfies the mathematic model only when the antenna is placed high enough with an ideal ground plane. However, trees, buildings, metal posts or power lines near the antenna and other non-idealness can result in large distortions in the antenna pattern. The pattern distortion is not a problem for the phased array, but may be vital in the amplitude-relied array discussed here. It has been pointed out that the pattern distortions of a CMA can result in large DF errors up to 15° and that using measured antenna patterns can effectively improve the quality of HF radar surface current maps [16–18]. For the same reasons mentioned above, we hope to find an automatic method to calibrate the antenna pattern distortions and the gain/phase errors using the unknown sources. Fortunately, the everlasting enormous backscattered signals from the sea surface make the iterative self-calibration feasible [19], which is attributed to: (i) use of patterns closer to the actual ones generally improves the DOA estimation, guaranteeing the convergence of the iteration; (ii) the randomness of the sea echoes in both spatial and temporal domains makes the pattern at each look angle have a chance to be involved and adjusted, making the method robust; and (iii) the nature of sea currents decides that most sea echo signals associated with a given Doppler frequency and a given range cell have only one DOA and we can screen them out by checking the eigenvalues of their auto-correlation matrixes, leading to accurate parameter estimations. This is a major point to be discussed in this paper.

The rest of the paper is organised as follows. Section 2 describes the pattern synthesis method based on adaptive interference suppression. Section 3 describes the iterative algorithm to estimate both the individual antenna patterns and the channel phase errors. Section 4 demonstrates the simulation results to show the validness of the proposed method and Section 5 gives the conclusion.

2 Pattern synthesis of a CM-ULA

The array pattern is synthesised with weights at each receive channel by

$$p(\theta) = \left|\boldsymbol{W}^{\mathrm{H}}(\theta_{\mathrm{d}})\boldsymbol{a}(\theta)\right| \tag{1}$$

where $\boldsymbol{W}(\theta_{\mathrm{d}})$ is the weight vector corresponding to the desired direction θ_{d}, $\boldsymbol{a}(\theta)$ is the steering vector at the direction θ and the superscript $^{\mathrm{H}}$ denotes complex transpose.

In the application of HFSWR in sea state monitoring, the echo signal at each antenna is the superposition of the echoes from all the angles across the illuminated sea surface, which have similar power except for the modulation by the directional sea wave spectra and the Doppler broadening according to the sea current profile. Therefore both the mainlobe beamwidth and the sidelobe level should be considered in the pattern synthesis. The BF with a conventional window, such as the Hamming, Hanning and Dolph–Chebyshev windows etc., cannot offer a satisfying mainlobe beamwidth for the application concerned here. Fortunately, the ABF method provides a convenient approach to solve this problem. The pattern can be optimised subject to the sidelobe and/or mainlobe constraints. The famous minimum variance distortionless response (MVDR), or the Capon method, minimises the array output power while maintaining unit response at the desired direction θ_{d} [20, 21], leading to the array weight vector

$$\boldsymbol{W}(\theta) = \frac{\boldsymbol{R}^{-1}\boldsymbol{a}(\theta)}{\boldsymbol{a}^{\mathrm{H}}(\theta)\boldsymbol{R}^{-1}\boldsymbol{a}(\theta)} \tag{2}$$

where $\boldsymbol{R}$ is the auto-correlation matrix of the array snapshots. The MVDR generates sidelobe nulls in the directions of the interferences, and the stronger the interference, the deeper the nulls. So, virtual interferences can be used to adjust the synthesised pattern [9]. When a large number of virtual interferences are uniformly spaced throughout the sidelobe region, the pattern can iteratively approach to the desired one by adjusting the interference powers.

In this paper, two CMA with the same normal direction are combined to form a CM-ULA, whose steering vector is given by

$$\boldsymbol{a}(\theta) = \boldsymbol{a}_e(\theta) \circ \boldsymbol{a}_a(\theta) \tag{3.1}$$

$$\boldsymbol{a}_a(\theta) = \left[1,\ 1,\ 1,\ \mathrm{e}^{\mathrm{j}\beta(\theta)},\ \mathrm{e}^{\mathrm{j}\beta(\theta)},\ \mathrm{e}^{\mathrm{j}\beta(\theta)}\right]^{\mathrm{T}} \tag{3.2}$$

where $\boldsymbol{a}_e(\theta) = [a_{e,1}(\theta),\ \ldots,\ a_{e,6}(\theta)]^{\mathrm{T}}$ is the element pattern vector, $\boldsymbol{a}_a(\theta)$ is the array synthesis vector, $\beta(\theta) = (2\pi\ d/\lambda)$ $\sin\ \theta$ is the spatial phase shift associated with θ, λ is the radar wavelength, d is the spacing, the operator $\circ$ denotes element multiplying and the superscript $^{\mathrm{T}}$ denotes transpose. In an ideal situation, we have

$$\boldsymbol{a}_e(\theta) = \left[1,\ \sin\left(\theta+\frac{\pi}{4}\right),\ \cos\left(\theta+\frac{\pi}{4}\right),\ 1,\ \sin\left(\theta+\frac{\pi}{4}\right),\ \cos\left(\theta+\frac{\pi}{4}\right)\right]^{\mathrm{T}} \tag{3.3}$$

Here, we choose a spacing of 0.75λ for discussion. The synthesised pattern using the above ABF method with a -20 dB sidelobe level constraint is shown in Fig. 1. The pointing direction is 0° and the mainlobe region is set from -20 to 20°. Totally 160 virtual interferences are uniformly spaced with a 2° spacing throughout the 360° look angles, except the mainlobe region. The superiority of the pattern synthesised by the ABF with the 2-unit CM-ULA over that by the matched CBF ($\boldsymbol{W}(\theta) = \boldsymbol{a}(\theta)$) with the same CM-ULA and that by the CBF with a 3-element ULA with a half-wavelength spacing is obvious. The sidelobe is greatly

doi: 10.1049/iet-rsn.2013.0141

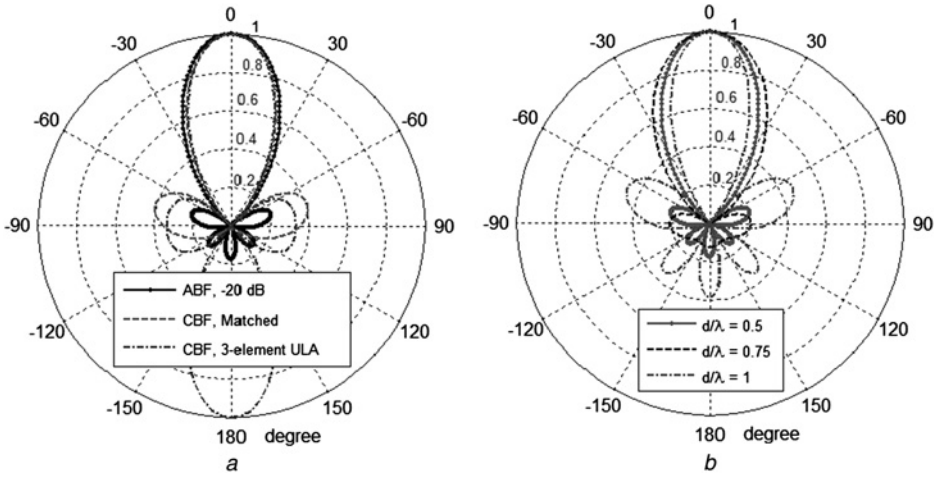

Fig. 1 *Synthesised patterns in the modulus sense using the ABF by the 2-unit CM-ULA*

a Comparison of the ABF pattern by the 2-unit CM-ULA (solid) with the matched CBF ($\boldsymbol{W}(\theta) = \boldsymbol{a}(\theta)$) by the same CM-ULA (dash), and the CBF by a 3-element ULA with a half-wavelength spacing (dash-dot)

b Comparison of ABF patterns by the 2-unit CM-ULA under different spacing-to-wavelength value, $d/\lambda = 0.75$ (solid), 0.5 (dash) and 1 (dash-dot)

decreased, and the front-to-back ratio is greatly increased as compared with the ULA, at a price of slightly increased mainlobe beamwidth. In the ABF pattern, the half beamwidth of the mainlobe is about 20° and the first sidelobe is about -14 dB. The selection of $d/\lambda = 0.75$ is a tradeoff of the mainlobe beamwidth and the sidelobe level. The beamwidth may still be somewhat large; however, such an array is quite attractive in the sea state monitoring. More flexible, non-uniform control of the sidelobe levels can also be used in the ABF pattern synthesis when there are sheltered regions. Proper relaxation of the constraints on the sidelobes can further reduce the mainlobe beamwidth. There are also more sophisticated pattern synthesis algorithms which provide efficient controls of both the mainlobe shaping and the sidelobe levels for arbitrary arrays, for example, that via optimisation of the weighted L_2 norm between desired and achieved patterns [22] and that via convex optimisation [23]. However, here we would not focus on the array pattern optimisation, but on the calibration of array errors, so we just choose the ABF-based algorithm as described in [9] for simplicity.

3 Calibration of the pattern and phase errors

In actual applications, the gains and phases of the receive channels (including the antennas and the receiver) are almost impossible to be made consistent, and they may vary slowing because of the active circuit components in the radar receiver and the loop antenna. Moreover, the antenna patterns almost always have distortions because of the non-idealness of the electromagnetic environment. Before the sea state extraction, the array errors including the antenna pattern distortions and the gain/phase errors should be calibrated to achieve a better BF performance. We would not like to resort to any known signals such as a transponder signal, but tend to estimate the errors from the sea echo signals. Fortunately, the sea echo signals consist of a large number of Bragg resonance echo signals from different directions of the sea surface, which normally have a signal-to-noise ratio (SNR) of 20–40 dB. These signals have different Doppler shifts corresponding to the current profile at the range cell concerned, thus making most of the signals have only one DOA, which provides high-quality sources for the calibration.

The radar receive signal model in the case of D sources with array errors can be denoted as

$$\begin{aligned}\boldsymbol{X}(t) &= \boldsymbol{\Phi G A}(\theta)\boldsymbol{S}(t) + \boldsymbol{N}(t)\\ &= \boldsymbol{\Phi G}[\boldsymbol{A}_e(\theta) \circ \boldsymbol{A}_a(\theta)]\boldsymbol{S}(t) + \boldsymbol{N}(t)\\ &= \boldsymbol{\Phi}\{[\boldsymbol{G A}_e(\theta)] \circ \boldsymbol{A}_a(\theta)\}\boldsymbol{S}(t) + \boldsymbol{N}(t)\end{aligned} \tag{4}$$

where $\boldsymbol{X}(t) = [x_1(t), \ldots, x_6(t)]^{\mathrm{T}}$ is the array snapshot vector, $\boldsymbol{S}(t) = [s_1(t), \ldots, s_D(t)]^{\mathrm{T}}$ is the source signal vector, $\boldsymbol{A}_e(\theta) = [\boldsymbol{a}_e(\theta_1), \ldots, \boldsymbol{a}_e(\theta_D)]^{\mathrm{T}}$ is the actual array response matrix corresponding to the source direction $\theta_k (k = 1, \ldots, D)$, $\boldsymbol{\Phi} = \mathrm{diag}\left[\mathrm{e}^{\mathrm{j}\varphi_1}, \ldots, \mathrm{e}^{\mathrm{j}\varphi_6}\right]$ and $\boldsymbol{G} = \mathrm{diag}[g_1, \ldots, g_6]$ are, respectively, the channel phase and gain matrix and $\boldsymbol{N}(t) = [n_1(t), \ldots, n_6(t)]^{\mathrm{T}}$ is the noise vector. The specific noise distribution does not have a great impact on the final result because only the spectral points with high enough SNR are to be involved in the following calculations. Without loss of generality we set $a_{e,1}(\theta) = 1$, $\phi_1 = 0$ and $g_1 = 1$. Now, the problem is to estimate $\boldsymbol{\Phi}$, $\boldsymbol{G}$ and $\boldsymbol{A}_e(\theta)$ from (4). If the array manifold matrix $\boldsymbol{A}(\theta)$ is already known by measurement, the problem is reduced to be the estimation of $\boldsymbol{\Phi}$ and $\boldsymbol{G}$. However, the more general case is considered here. In fact, the estimation of the product of the channel gain and the individual antenna pattern, say $\boldsymbol{B}(\theta) = \boldsymbol{G A}_e(\theta)$, is enough for the consequent processing. So in the following, we will refer to $\boldsymbol{B}(\theta)$ as the antenna pattern without distinction.

Utilising the inherent co-phase property of the CMA, we can first simplify the calibration by modifying the channel phases inside the sub-array to make them consistent in phase. The channel phase matrix can be written as the product of the phase matrixes inside and across the sub-arrays

$$\boldsymbol{\Phi} = \boldsymbol{\Phi}_1 \boldsymbol{\Phi}_{41} \tag{5}$$

where $\boldsymbol{\Phi}_1 = \mathrm{diag}\left[1, \mathrm{e}^{\mathrm{j}\phi_{21}}, \mathrm{e}^{\mathrm{j}\phi_{31}}, 1, \mathrm{e}^{\mathrm{j}\phi_{54}}, \mathrm{e}^{\mathrm{j}\phi_{64}}\right]$ with $\phi_{m1} = \phi_m - \phi_1 (m = 2, 3)$ and $\phi_{m4} = \phi_m - \phi_4 (m = 5, 6)$ and $\boldsymbol{\Phi}_{41} = \mathrm{diag}\left[1, 1, 1, \mathrm{e}^{\mathrm{j}\phi_{41}}, \mathrm{e}^{\mathrm{j}\phi_{41}}, \mathrm{e}^{\mathrm{j}\phi_{41}}\right]$. $\boldsymbol{\Phi}_1$ can be easily estimated by calculating the cross-correlation coefficient of the Doppler spectral values on the associated channels.

Here by Doppler spectral we mean the complex Fourier transform of the temporal sequence. Select a set of high SNR (typically >20 dB) Doppler spectral points at the nearby range cells, namely $\boldsymbol{Y}_q = [y_{1,q}, \ldots, y_{6,q}]^{\mathrm{T}} (q = 1, \ldots, Q)$, then $\phi_{mk}((m, k) \in \{(2, 1), (3, 1), (5, 4), (6, 4)\})$ can be estimated by

$$\hat{\phi}_{mk} = \arg\left\{\frac{1}{Q}\sum_{q=1}^{Q} Y_{m,q} Y_{k,q}^{*}\right\} \tag{6}$$

ϕ_{41} cannot be directly calculated by the phase difference between the spectra at channels #4 and #1 because the spacing between the two CMA has introduced an extra phase term, $(2\pi d/\lambda)\sin\theta$. This direction-dependent term should be removed, which requires the estimation of the DOA θ. It is a key point in the whole calibration process.

Now the modified version of the array receive signal is

$$\boldsymbol{X}'(t) = \hat{\boldsymbol{\Phi}}_1^{*}\boldsymbol{X}(t) = \hat{\boldsymbol{\Phi}}_1^{*}\boldsymbol{\Phi}[\boldsymbol{B}(\theta) \circ \boldsymbol{A}_a(\theta)]\boldsymbol{S}(t) + \boldsymbol{N}'(t) \tag{7}$$

with $\boldsymbol{N}'(t) = \hat{\boldsymbol{\Phi}}_1^{*}\boldsymbol{N}(t)$ and the superscript * denotes complex conjugate. A novel algorithm is proposed to automatically estimate the actual antenna pattern $\boldsymbol{B}(\theta)$ and the phase ϕ_{41} in an iterative way, which is described as follows.

Initialisation: set the antenna patterns to be ideal according to (3.3), $\boldsymbol{\Phi} = \boldsymbol{I}$, $\boldsymbol{G} = \boldsymbol{I}$ and calculate $\boldsymbol{B}(\theta)$.

Step 1: Select a set of high-SNR spectral points as candidate calibration sources. For each spectral point, form the array snapshots $\boldsymbol{Y}_q(t)(q = 1, \ldots, Q)$ using a moving window, calculate the auto-correlation matrix in the spatial domain, $\boldsymbol{R}_{YY} = E[\boldsymbol{Y}_q(t)\boldsymbol{Y}_q^{\mathrm{H}}(t)]$ ($E[\cdot]$ denotes mathematic expectation), and execute an eigenvalue decomposition to obtain the eigenvalues $\lambda_m (m = 1, \ldots, 6)$ in descending order. Further screen out the single-DOA spectral points, namely $\bar{\boldsymbol{Y}}_q(t)\big(q = 1, \ldots, Q_1\big)$, by checking the steepest descent criterion, that is, $(\lambda_1/\lambda_2) > ((\lambda_m)/\lambda_{m+1})(m = 2, \ldots, 5)$ and $(\lambda_1/\lambda_2) > 10$.

Step 2: For the q'th calibration point, construct loop-relative-to-monopole snapshots to remove the phase error between the two CMAs by

$$\boldsymbol{X}''(t) = \left[\frac{x_2'(t)}{x_1'(t)}, \frac{x_3'(t)}{x_1'(t)}, \frac{x_5'(t)}{x_4'(t)}, \frac{x_6'(t)}{x_4'(t)}\right]^{\mathrm{T}} \tag{8}$$

The corresponding relative steering vector associated with θ is

$$\boldsymbol{b}''(\theta) = \left[\frac{\hat{b}_2(\theta)}{\hat{b}_1(\theta)}, \frac{\hat{b}_3(\theta)}{\hat{b}_1(\theta)}, \frac{\hat{b}_5(\theta)}{\hat{b}_4(\theta)}, \frac{\hat{b}_6(\theta)}{\hat{b}_4(\theta)}\right]^{\mathrm{T}} \tag{9}$$

where $\hat{b}_m(\theta)(m = 1, \ldots, 6)$ is the estimated antenna pattern used in the current step and $\hat{b}_1(\theta) = 1$. As for the single-DOA source, the signal model becomes

$$\boldsymbol{X}''(t) = \boldsymbol{b}''(\theta)s(t) + \boldsymbol{N}''(t) \tag{10}$$

Use the conventional Multiple signal classification algorithm [24] to obtain an estimation of the DOA, $\hat{\theta}_q$.

Step 3: Calculate $\hat{\phi}_{41}$ via

$$\hat{\phi}_{41} = \arg\left\{\frac{1}{Q_1}\sum_{k=1}^{Q_1} \bar{Y}_{4,q}\bar{Y}_{1,q}^{*}\mathrm{e}^{-\mathrm{j}\beta\left(\hat{\theta}_q\right)}\right\} \tag{11}$$

Step 4: For each look angle θ, find all the spectral points falling on it, and calculate the median value

$$r_m = \mathrm{median}\left\{\left|\frac{\bar{Y}_{m,q}}{\bar{Y}_{1,q}}\right|\big(q = 1, \ldots, Q_{1,\theta}\big)\right\}$$

then adjust the antenna pattern via

$$\hat{b}_m^{(l)}(\theta) = (1 - \mu)\hat{b}_m^{(l-1)}(\theta) + \mu r_m \mathrm{sgn}\big[a_{e,m}(\theta)\big] \tag{12}$$

for $m = 2, \ldots, 6$, where l is the iteration index, μ is the learning rate between 0 and 1 and sgn[·] is the sign operator.

Step 5: Check whether the estimated antenna pattern satisfies the convergence criterion, that is

$$\varepsilon_m^{(l)} = \sqrt{\frac{1}{N_\theta}\sum_{\theta}\left|\hat{b}_m^{(l)}(\theta) - \hat{b}_m^{(l-1)}(\theta)\right|^2} \le \gamma \quad \text{for all} \quad m \tag{13}$$

where $\varepsilon_m^{(l)}$ is the root-mean-square error (RMSE) between the estimated pattern of antenna m in the l'th and $(l-1)$'th recursions, N_θ is the number of look angles in the calculation and γ is the preset threshold. If true, the iteration is terminated, otherwise go to step 1 to continue the iteration.

Finally, we obtain the estimations of the individual antenna patterns and the phase errors, which can be used in both the DF and BF processes for a better performance.

4 Simulation results

Simulations were executed to evaluate the performance of the proposed method for calibration. The tide-driven current model was used to simulate the radar echoes received by a two-set CMA-ULA. For simplicity, a uniform current field of 1 m/s was adopted, whose direction changes 2° clockwise in each data frame of about 8 min. The wind direction was set to be constantly 60° relative to the north. The radar look angle was set to be from −90 to 90° to guarantee there were sufficient one-DOA sources, whereas the situation that the radar is surrounded with sea waters was not considered here. Each 2.5 km range cell was separated into 900 small cells with a dimension of 500 m by 1°. The echo signals on the small cells were simulated according to the Barrick's first-order scattering theory [25], multiplied by the individual antenna directional coefficients and the receiver channel gain and phase factors, and then summed to give the final receive signals [26]. Each antenna pattern was controlled by 19 equally spaced points with a random variation factor between 0.2 and 2. Each channel had a random phase and a gain factor between −3 and 3 dB. The simulated Doppler power spectrum on Channel 1 is shown in Fig. 2, where the calculated noise level and the threshold for selecting candidate spectral points for the calibration are also indicated.

The proposed algorithm was executed to calculate the distorted patterns and the phase errors. One data sequence of 1024 samples, which contains echo signal from only one range cell, was processed in each iteration. This was a relatively poor condition since there are usually many range cells ready to be used. Two hundred iterations were run. The result RMSE between the estimated and the actual patterns, and those between the estimated patterns in successive iterations are shown in Figs. 3*a* and *b*, respectively. The downward trend of the RMSE is obvious,

doi: 10.1049/iet-rsn.2013.0141

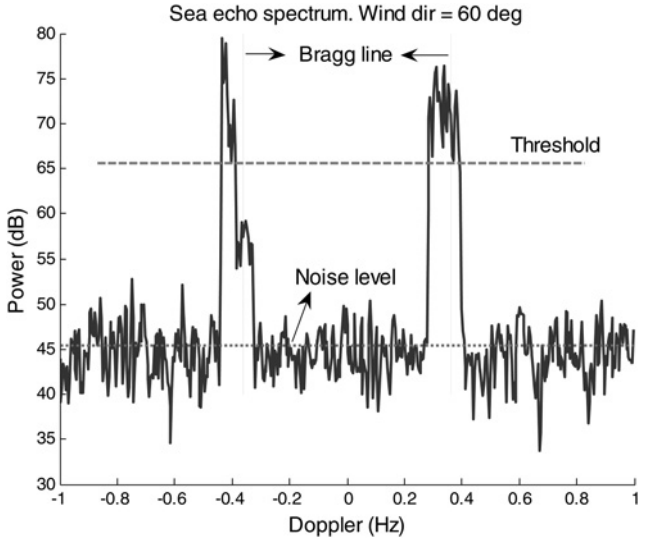

Fig. 2 *Simulated Doppler power spectrum on Channel 1, with the calculated noise level plotted in the red dotted line and the threshold for candidate spectral points in the purple dashed line*

The radial current profile here is $v = \cos(\theta - 150°)$m/s

particularly in the first few iterations, but there are two rising intervals indexed from 45 to 55 and from 135 to 145. Note that in the simulation the current direction was $\theta_{cur} = 2k - 90(k = 0, \ldots, 199)°$ and the radial current profile was $v(\theta) = \cos(\theta - \theta_{cur})$ (as shown in Fig. 4), the large proportions of two-DOA sources (say larger than 80%) in the two intervals led to the rises of the RMSE. However, if we choose a RMSE threshold of −3 dB for the decision of convergence, we can already obtain a good result. The estimated patterns in the two CMA coincide with the actual patterns very well, which are shown in Figs. 5*a* and *b*, respectively. Fig. 6 shows the estimated phase errors between the loops and monopole inner each CMA and the phase error across the CMA (that is, between the two monopoles). The inner-CMA phase errors are easy to estimate, whereas the across-CMA phase error is relatively difficult, as can be seen from Fig. 6. In this sense, the convergence of the estimated phase error can be regarded as an important indicator of the calibration performance. When the single-DOA spectral points make up a larger proportion of all the candidate ones, the error of the estimation of across-CMA phase error, ϕ_{41}, is very small, but when the number of single-DOA points decreases to be quite small, say below 20%, the error becomes big. The big-error intervals are the same as those shown in Fig. 3*b*. This once again shows that the large number of single-DOA sources is one of the key factors of the calibration algorithm. Fortunately, such a condition is often satisfied because of the nature of the sea surface current, that is, except for the application on an islet, the coastal currents often flow nearly parallel to the coastline, resulting in a desirable radial velocity profile. By simulations we found that a moderate SNR, namely 20 dB, is enough to achieve a satisfactory result, so in real applications a large number of spectral points can be used for the calibration. Here it should be pointed out that this SNR condition can be easily achieved by a modern HFSWR. Our experience of field experiment has shown that the SNR of the Bragg peaks at nearby range cells often exceeds 40 dB with an average power of 100 W under a slight sea scale. We also found that the initial conditions of the current velocity profile have no obvious effects on the final results, which shows the robustness of the proposed method.

Finally, the array errors were calibrated in the pattern synthesis process. The synthesised patterns pointing to 0° before and after the calibration are shown in Fig. 7. As can be seen, the great distortions of the synthesised pattern have been effectively corrected.

In the above simulation, the SNR of the first-order Doppler spectral peak was about 30 dB. When the SNR decreases, larger calibration errors occur. By the simulation we find that the method may fail when the SNR is lower than 15 dB. The level of the element pattern distortion is another factor that has impact on the calibration accuracy. Generally larger distortions (not only a shrink or amplification) lead to less accurate calibration values. The standard error of the estimated across-CMA phase error, ϕ_{41}, against pattern distortion level under different SNR by statistic simulation is shown in Fig. 8. Since here the antenna patterns and

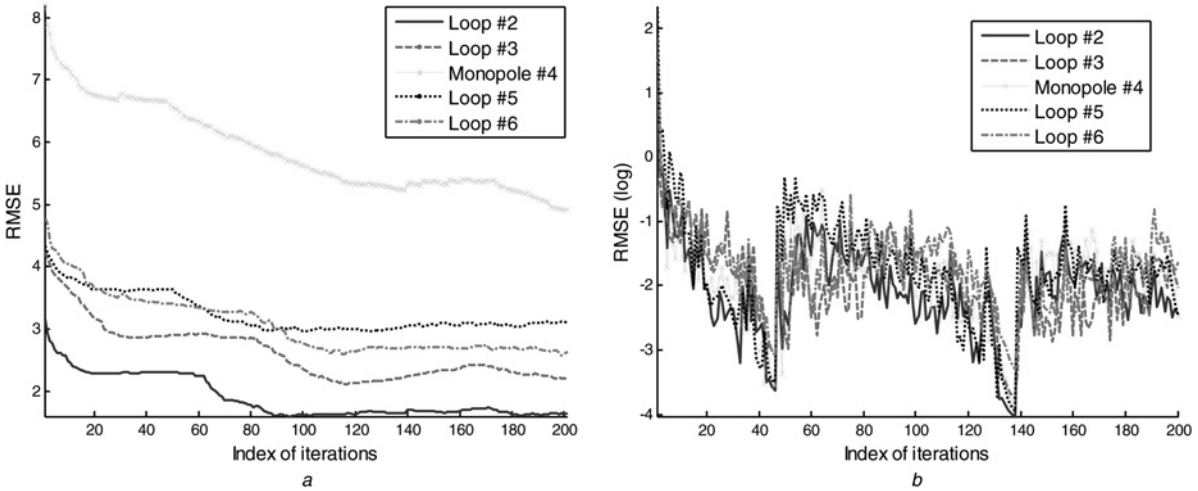

Fig. 3 *Result RMSE between the estimated and the actual patterns, and those between the estimated patterns in successive iterations*

a RMSE between the estimated and actual patterns
b RMSE between patterns in successive iterations

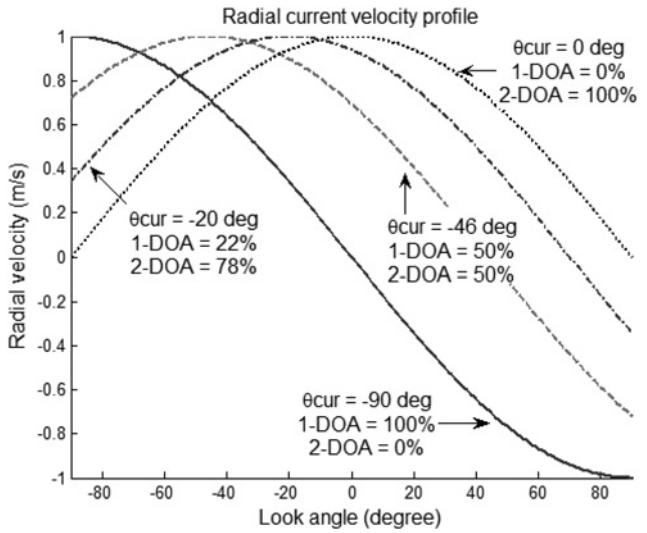

Fig. 4 *Radial current profiles with different current directions*
Different proportions of single-DOA and two-DOA sources result correspondingly

channel gains are considered as a whole, a rough balance of the signals on each channel by the total energy is necessary before the iteration starts.

Some other simulations were also done to make clear how different proportions of the single-DOA sources among the total spectral points affect the calibration performance. For this purpose, the current directions were set constantly in the iterations, which result in different proportions of single- and two-DOA sources correspondingly. For example, the current directions of ±90, ±45, ±20 and 0° correspond to proportions of 100, 50, 22 and 0% for the single-DOA sources, respectively, similar as shown in Fig. 4. Satisfactory calibration results are achieved when the proportion of single-DOA sources is $>20\%$, or equivalently the current direction is between -160 and $-20°$ or between 20 and 160°. Nevertheless, only the patterns on the arc regions containing the single-DOA sources can be approached, whereas those on the regions with two-DOA sources cannot. However, in realities the

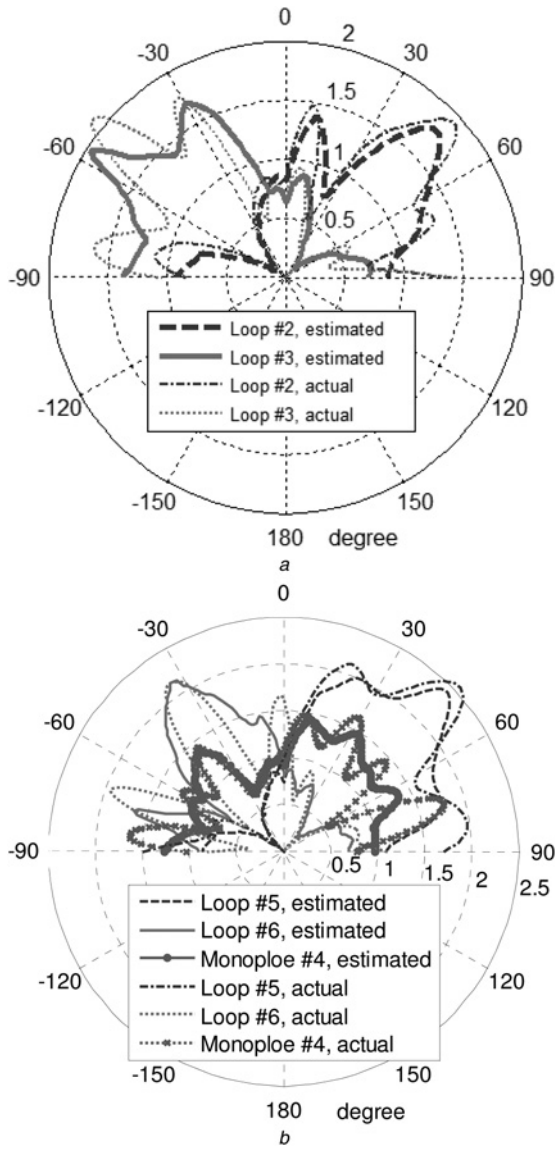

Fig. 5 *Estimated patterns in the modulus sense in*
a CMA 1
b CMA 2

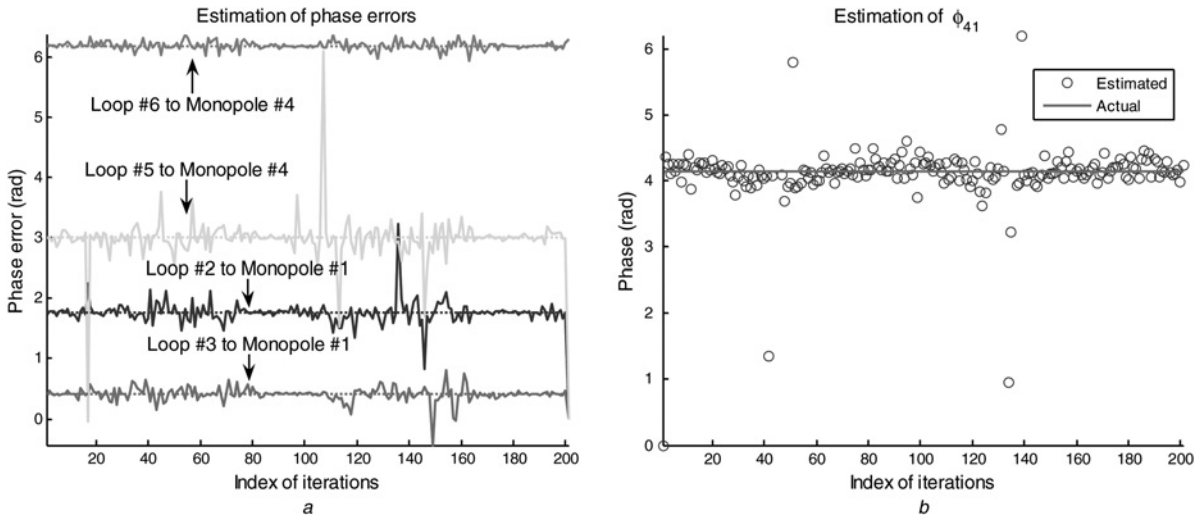

Fig. 6 *Estimated phase errors between the loops and monopole inner each CMA and the phase error across the CMA*
a Estimated phase errors between the loops and the monopole inner the CMAs
b Phase error across the CMA, ϕ_{41}

doi: 10.1049/iet-rsn.2013.0141

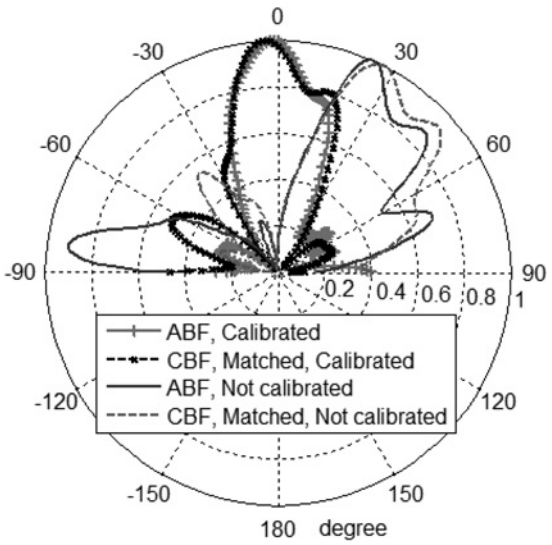

Fig. 7 *Synthesised pattern in the modulus sense with and without calibration*

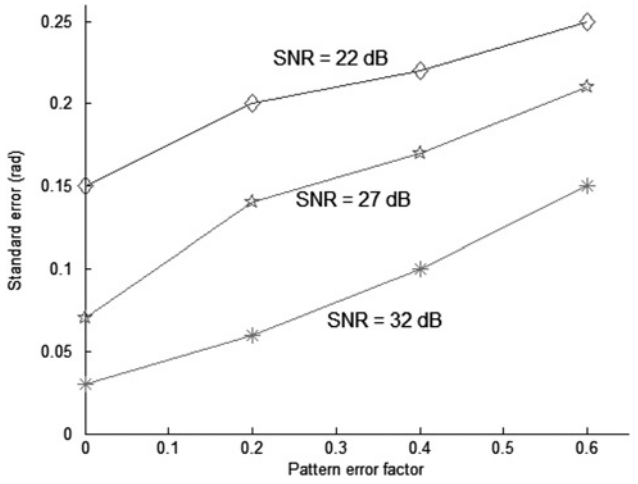

Fig. 8 *Standard error of the across-CMA phase difference, ϕ_{41}, under different SNR*

Pattern error factor, r, is used to control the pattern distortion, that is, the 19 equally spaced samples of the patterns are calculated by the ideal values multiplied with random factors between $1+r$ and $1-r$ to give the final patterns by interpolation

current field is always varying, so patterns at every angular cell may get a chance to be calibrated. The number of single-DOA sources is seldom a problem in most situations unless the radar is surrounded by the sea. Therefore the proposed method is capable of calibrating the array errors in rather wide situations.

5 Conclusions

In this paper, we combined the CMA and ULA to form a two-unit CM-ULA for the application of the sea state monitoring HFSWR, and proposed a novel iterative algorithm to calibrate the array errors, including the antenna pattern distortions and channel gain/phase errors. Simulations were executed and the results showed the effectiveness of the method. The method relies on a large number of single-DOA sources mainly from the first-order Doppler spectral regions. Although this condition is often satisfied in real applications and the corresponding calibration process is relatively easy to realise, further work should be done to solve the calibration problem in the more general case allowing use of arbitrarily multiple sources, and to finally solve the calibration problem in the omni-directional detection applications.

6 Acknowledgments

This work was supported by the Ocean Public Welfare Scientific Research Project under grant 201205032-3, the National Natural Science Foundation of China under grant 61371198 and the Natural Science Foundation of Jiangsu Province, China under grant SBK201240419.

7 References

1 Wyatt, L.R.: 'Use of HF radar for marine renewable applications'. OCEANS 2012, Yeosu, 21–24 May 2012, doi: 10.1109/OCEANS-Yeosu.2012.6263439, pp. 1–5
2 Shen, W., Gurgel, K.-W., Voulgaris, G., *et al.*: 'Wind speed inversion from HF radar first-order backscatter signal'. Ocean Dynamics, 11 August 2011, doi: 10.1007/s10236-011-0465-9, pp. 1–17
3 Abascal, A.J., Castanedo, S., Fernandez, V., Ferrer, M.I., Medina, R.: 'Oil spill trajectory forecasting and backtracking using surface currents from high-frequency (HF) radar technology'. OCEANS 2011, Santander, Spain, 6–9 June 2011, doi: 10.1109/Oceans-Spain.2011.6003575, pp. 1–8
4 Barrick, D., Lipa, B.: 'Japan tsunami detected by HF radars on two continents'. OCEANS 2011, Waikoloa, HI, 19–22 September 2011, pp. 1–5
5 Lipa, B.J., Barrick, D.E.: 'Least-squares method for the extraction of surface currents from CODAR crossed-loop data: application at ARSLOE', *IEEE J. Ocean. Eng.*, 1983, **8**, (4), pp. 226–253
6 Frolov, S., Paduan, J., Cook, M., Bellingham, J.: 'Improved statistical prediction of surface currents based on historic HF-radar observations', *Ocean Dyn.*, 2012, **62**, (7), pp. 1111–1122
7 Helzel, T., Kniephoff, M., Petersen, L., Mariette, V., Thomas, N.: 'Accuracy and reliability of ocean radar WERA in beam forming or direction finding mode'. Proc. 2011 IEEE/OES 10th Current, Waves and Turbulence Measurements (CWTM), Monterey, CA, 20–23 March 2011, doi: 10.1109/CWTM.2011.5759518, pp. 21–24
8 Helzel, T., Hansen, B., Kniephoff, M., Petersen, L., Valentin, M.: 'Introduction of the compact HF radar WERA-S'. Proc. 2012 IEEE/OES Baltic Int. Symp. (BALTIC), Klaipeda, 8–10 May 2012, doi: 10.1109/BALTIC.2012.6249215, pp. 1–3
9 Olen, C.A., Compton Jr R.T.: 'A numerical pattern synthesis algorithm for arrays', *IEEE Trans. Antennas Propag.*, 1990, **38**, (10), pp. 1666–1676
10 Bourdillon, A., Delloue, J.: 'Phase correction of an HF multireceiver antenna array using a radar transponder'. IEEE Int. Conf. ICASSP-94, Adelaide, SA, 19–22 April 1994, vol. 6, pp. 125–128
11 Solomon, I.S.D., Gray, D.A., Abramovich Yu, I., Anderson, S.J.: 'Over-the-horizon radar array calibration using echoes from ionised meteor trails', *IEE Proc. Radar Sonar Navig.*, 1998, **145**, (3), pp. 173–180
12 Fabrizio, G.A., Gray, D.A., Turley, M.D.: 'Using sources of opportunity to compensate for receiver mismatch in HF arrays', *IEEE Trans. Aerosp. Electron. Syst.*, 2001, **37**, (1), pp. 310–316
13 Kim, J., Yang, H.J., Jung, B.W., Chun, J.: 'Blind calibration for a linear array with gain and phase error using independent component analysis', *IEEE Antennas Wirel. Propag. Lett.*, 2010, **9**, pp. 1259–1262
14 Liu, A., Liao, G., Zeng, C., Yang, Z., Xu, Q.: 'An eigenstructure method for estimating DOA and sensor gain-phase errors', *IEEE Proc. Trans. Signal Proc.*, 2011, **59**, (12), pp. 5944–5956
15 Zhang, Y., Ma, H., Tan, P.: 'A low complexity calibration method of gain and phase error for arrays with arbitrary geometry'. Proc. 2011 Int. Conf. Multimedia Technology (ICMT), Hangzhou, China, 26–28 July 2011, doi: 10.1109/ICMT.2011.6001803, pp. 3342–3345
16 Barrick, D.E., Lipa, B.J.: 'Using antenna patterns to improve the quality of SeaSonde HF radar surface current maps'. Proc. IEEE Sixth Working Conf. Current Measurement, 1999, San Diego, CA, 11–13 March 1999, pp. 5–8

17 Kohut, J.T., Glenn, S.M.: 'Improving HF radar surface current measurements with measured antenna beam patterns', *J. Atmos. Ocean. Technol.*, 2003, **20**, pp. 1303–1316
18 Paduan, J.D., Kim, K.C., Cook, M.S., Chavez, F.P.: 'Calibration and validation of direction-finding high-frequency radar ocean surface current observations', *IEEE J. Ocean. Eng.*, 2006, **31**, (4), pp. 862–875
19 Zhou, H., Wen, B.: 'Automatic antenna pattern estimation for high-frequency surface wave radars', *J. Electromagn. Waves Appl.*, 2013, **27**, (2), pp. 168–179
20 Capon, J.: 'High-resolution frequency-wavenumber spectrum analysis', *IEEE Proc.*, 1969, **57**, (8), pp. 1408–1418
21 Haykin, S., Kumaresan, R.: 'Array signal processing' (Prentice-Hall, NJ, 1985)
22 Zhou, P.Y., Ingram, M.A.: 'Pattern synthesis for arbitrary arrays using an adaptive array method', *IEEE Trans. Antenna Propag.*, 1999, **47**, (5), pp. 862–869
23 Lebret, H., Boyd, S.: 'Antenna array pattern synthesis via convex optimization', *IEEE Trans. Signal Process.*, 1997, **45**, (3), pp. 526–572
24 Schmidt, R.O.: 'Multiple emitter location and signal parameter estimation', *IEEE Trans. Antennas Propag.*, 1986, **Ap-34**, (3), pp. 276–280
25 Barrick, D.: 'First-order theory and analysis of MF/HF/VHF scatter from the sea', *IEEE Trans. Antennas Propag.*, 1972, **20**, (1), pp. 2–10
26 Laws, K., Fernandez, D.M., Paduan, J.D.: 'Simulation-based evaluations of HF radar ocean current algorithms', *IEEE J. Ocean. Eng.*, 2000, **25**, (4), pp. 481–491

doi: 10.1049/iet-rsn.2013.0141